Flexible Power Control for Stand-alone Interlinking Converter in PV and Storage System Application

Zhongting Tang, Ariya Sangwongwanich, and Frede Blaabjerg
AAU Energy, Aalborg University, Aalborg 9220, Denmark
E-mails: zta@et.aau.dk, ars@energy.aau.dk, fbl@et.aau.dk

***Abstract*—The stand-alone interlinking converter is promising in residential PV systems due to its multiport, high power density, multifunction and power control flexibility. To exhibit the multifunction of the stand-alone interlinking converter, this paper proposes a flexible power control strategy with changeable operations. After configuring the grid-connected PV and storage system with the stand-alone converter, a flexible control method is proposed to enable the stand-alone converter to act as a DC-DC converter, a single-phase inverter, or an interlinking converter. In that case, the PV and storage system can flexibly operate under the PV+Battery mode, the Battery+Grid mode, and the PV+Battery+Grid mode. Experiments have been carried out on a hybrid grid-connected PV and storage system to validate the good performance in terms of versatility and flexible power controllability of the proposed control strategy.**

***Index Terms*—Flexible power control, Grid-connected, Multifunction, Stand-alone hybrid converter, Photovoltaic and storage system**

I. Introduction

Integrating the storage battery has become the favorite solution in smart grid-connected PV systems, where there are many commercial PV and storage products, e.g., the SEXXXXH series in Solaredge, and the Sunny Boy Storage series in SMA [1]. However, most of them are composed of several separate converters connected in parallel at DC or AC buses [2], [3]. For example, an inverter and a bidirectional DC-DC converter are connected in parallel to interface the PV, the battery and the utility grid. Furthermore, the inverter for the PV always adopts two-stage converters to achieve wide voltage gain and increase energy harvesting.

Generally, the multiple conversion stages increase system cost, and decrease power density as well as reliability [3]. By comparison, stand-alone converters can provide multiport and high compactness, which are more suitable for the renewable distributed system [4], [5]. Among them, high-frequency transformer-based multiport converters, i.e., solid-state transformer converters, are favorite in hybrid microgrids to connect the renewables, DC and AC loads [4]. Such isolation multiport converter has less harmonic influence among each port, yet compromises in terms of systems cost and volume compared to the transformerless one [5]. For instance, literature [5] proposed a transformerless stand-alone interlinking converter structure with low leakage current, high compactness, and flexible power controllability.

This work was supported by the Novo Nordisk Fonden through the Interdisciplinary Synergy Programme (Award Ref. No.: NNF18OC0034952).

As to the control strategy, the control objective of the multiport converter can be classified into the primary converter level and the secondary system level. The primary control focuses on power quality and flexible power controllability, while the secondary control mainly considers coordination and optimal power management [6], [7]. There is an amount of research on basic control methods for the power quality, such as proportional-integral (PI), proportional-resonance (PR), repetitive-controller (RC), advanced slide mode controller, observed emulation-based controller, and so on [6], [8]. The system level control in hybrid microgrids is almostly based on droop control methods [7], [9]. However, when applied in grid-connected renewable systems, extra demands are required, e.g., synchronous with the grid, flexible power control to support the grid, and also optimal self-consumption. That means such a PV system should own all characteristics met for the grid-connected and off-grid operations. As presented in [10], the bidirectional interlinking converter can operate as current/voltage sources under the ON/OFF grid conditions. In [11], a flexible power controller is developed to support ancillary and intelligent services in PV systems, like low voltage ride-through (LVRT), flexible active and reactive power regulation, and reliability oriented thermal control.

In the grid-tied application, the current source control is more preferred for the power management, which is still valid in the stand-alone interlinking converter. Compared to the typical interlinking converter, the control method for the stand-alone converter can be easier for less conversion stages and fewer power devices. The stand-alone interlinking converter concept has been validated in ref [6] and its derived topology [12], which has high power efficiency, low leakage current without any physical transformer, flexible power control capability as well as simultaneous DC and AC outputs. An exemplified derived hybrid converter has already been proposed in [12] as well as the operation modes and the dedicated modulation method. This paper thus focuses on the figuration of the flexible power control scheme for such type converters.

To demonstrate the application of the stand-alone interlinking converter, this paper proposes a flexible power control strategy along with the configuration of a grid-connected hybrid PV system, interfacing the PV, the battery, and the grid. Three operation modes have been introduced with the proposed control strategy to verify the multifunction and power control flexibility. The rest organization is in the following. Section II presents the interlinking converter prototype and

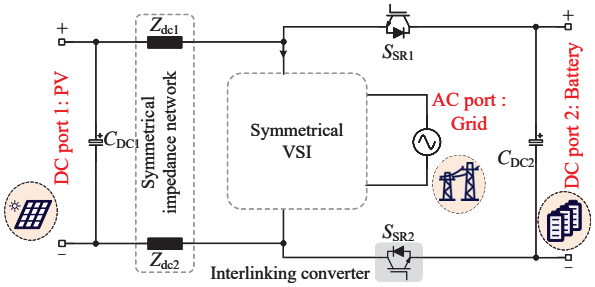

Fig. 1. Stand-alone interlinking converter proposed in [6], where VSI is the abbreviation of voltage source inverter, $S_{SR1\text{-}2}$ are the synchronous rectifier switches, $Z_{dc1\text{-}2}$ are the symmetrical impedance, and $C_{DC1\text{-}2}$ are the DC port capacitors, respectively.

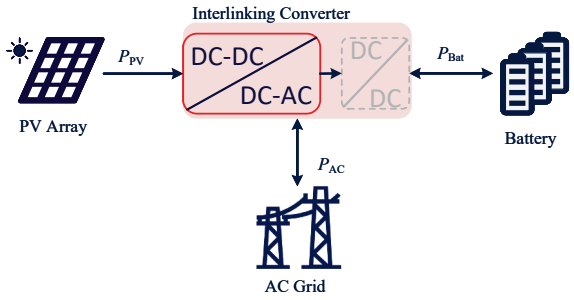

Fig. 2. Power flow of the grid-connected PV and storage system, where P_{PV}, P_{Bat} and P_{AC} are the PV produced power, the battery power and the grid power, respectively.

the configuration of the grid-connected hybrid PV system. Then, the basic control strategy and mode switching scheme are introduced in Section III. In Section VI, experiments are carried out on a stand-alone interlinking PV converter system to demonstrate three operation modes. Finally, the conclusion is given in Section V.

II. Hybrid System Configuration

A. Interlinking converter structure

As shown in Fig. 1, the stand-alone interlinking converter consists of a symmetrical impedance network, a symmetrical voltage source inverter (VSI), and a symmetrical synchronous rectifier switches ($S_{SR1\text{-}2}$). There are three ports (i.e., two DC ports and one AC port), where both two DC ports can connect to the PV with a low leakage current or connect to a storage battery. In this configuration, DC port 1 is connected to the PV array, DC port 2 connects to a battery set, and the AC port connects to the utility grid. When taken the symmetrical VSI as a single power switch, the stand-alone hybrid converter operates as a DC-DC converter. The hybrid converter can perform the DC-AC conversion when it acts as a normal voltage source inverter, and also implement both the DC-DC and DC-AC conversions simultaneously. In that case, such an interlinking converter has multifunction characteristics.

B. Configuration

A hybrid PV system configuration, including the PV array, the utility grid and the battery, is taken as an example to demonstrate the application of the interlinking converter, as shown in Fig. 2. Since the interlinking converter in Fig. 1 acts as a boost DC-DC converter when the VSI operates as a power switch, an extra DC-DC converter can be added at DC port 2 to achieve a wide voltage range for the battery, as presented as the gray part in Fig. 2.

C. Steady-state gains

Literature [12] has introduced that both the DC-DC conversion and the inversion can be finished in one switching cycle, leading to a limit between the DC-DC gain and the DC-AC modulation index. Therefore, a Z-source impedance is adopted as the symmetrical impedance network in the stand-alone interlinking converter system configuration to alleviate this problem. Correspondingly, the DC-DC gain can be expressed as

$$\frac{V_{DC}}{V_{PV}} = \frac{1}{1-2d} \tag{1}$$

where V_{DC} is the DC-link voltage, V_{PV} is the PV output voltage, and d is the short-through duty cycle. As the DC-DC and DC-AC conversions should be finished in one switching cycle, there is a limit between d and the inversion modulation signal m_{ac}, expressed as

$$d + m_{ac} \leq 1 \tag{2}$$

$$V_{ACpeak} = V_{PV}(1 + \frac{d}{1-2d}) \tag{3}$$

where V_{ACpeak} is the peak value of the grid voltage v_{ac}. In theory, V_{ACpeak} can be infinite if d is large enough, which can eliminate the limited DC-DC and DC-AC gains mentioned in [6]. However, d and m_{ac} should be designed considering the cost-effectiveness of the physical inductor and capacitor, and the voltage stress of the power switches (i.e., general characteristics considered in traditional DC-DC and DC-AC converters).

In addition, the conversion DC gain between V_{DC} and the battery voltage V_B can be given as

$$\frac{V_{DC}}{V_B} = \frac{1}{1-d} \tag{4}$$

The above system configuration shows that the introduced hybrid PV system has wide voltages range at each port.

III. Control Strategy

A. Control Block

Fig. 3 depicts the entire structure of the PV and storage system, where the symmetrical impedance adopts a Z-source impedance, a HERIC inverter is employed as the symmetrical VSI, and a symmetrical synchronous rectification DC-DC converter is adopted as the extra bidirectional DC-DC converter between DC port 2 and the battery to have a wide voltage range regulation. The HERIC inverter contains 6 IGBTs $S_{1\text{-}6}$ with antiparallel diodes, and two L-type filter ($L_{ac1,\,2}$). With the dedicated modulation method in [12], the

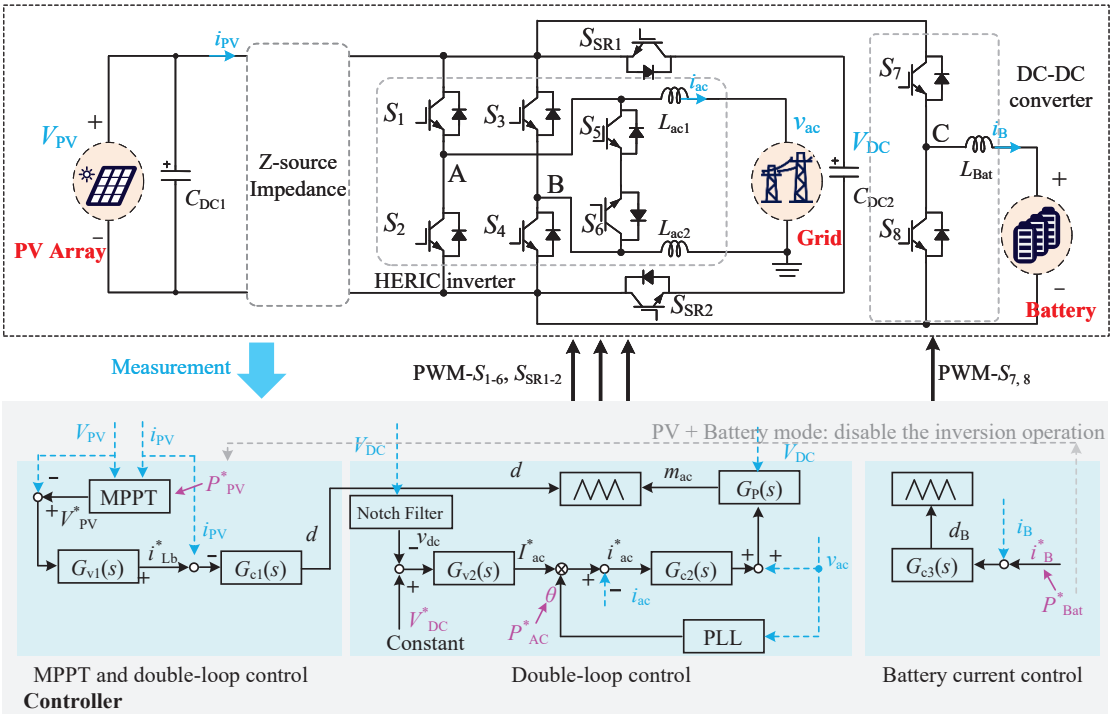

Fig. 3. Schematic and control block of the hybrid PV system.

interlinking converter can enable reactive power injection. The bidirectional DC-DC converter consists of two switches $S_{7\text{-}8}$ and one boost inductor L_{Bat}. Besides, i_{PV}, i_{ac}, and i_{B} represent the PV output current, the grid current, and the battery current, respectively. In addition to the multiplexing function of $S_{1\text{-}6}$, the DC-link capacitor can also be simultaneously employed as the output capacitor of DC-DC conversions in both the PV and battery sides.

The basic control for the hybrid PV system can be separated into three parts, i.e., the MPPT algorithm [8] with the double-loop control at the PV side, the double-loop control at the grid side, and the current control at the battery side, as shown in Fig. 3. The duty cycle d is the output signal of the controller at the PV side, m_{ac} is the modulation signal of the inversion generated from the double-loop controller at the grid side, and d_{B} is the duty cycle ratio generated by the current controller of the bidirectional DC-DC converter at the battery side. Those three controllers can be clarified in the following:

(1) Referring to the PV side controller in Fig. 3, the reference PV voltage V_{PV}^{*} is achieved through the MPPT control, e.g., the P&O algorithm, where the input sampling parameters are V_{PV} and i_{PV}. It should be noted that the MPPT control can be enabled or disabled under different operation modes. Then, a proportional-integral (PI) controller $G_{\text{v1}}(s)$ is adopted to generate the inductor current reference i_{PV}^{*}. Finally, another PI controller $G_{\text{c1}}(s)$ is employed in the inner current loop to achieve the short-through duty cycle d, which can be expressed as $\frac{V_{\text{DC}}}{V_{\text{PV}}} = \frac{1}{1-2d}$.

(2) Similarly, the double-loop controller [13] of the inversion at the grid side can also be flexibly controlled under different operation modes. As presented as the middle controller in Fig. 3, when the system operates in the grid-connected mode, the DC-link voltage V_{DC} is controlled by the inversion, where the reference DC-link voltage V_{DC}^{*} is set to be a constant value. The reference AC output current is obtained by a PI controller $G_{\text{v2}}(s)$ of the DC-link voltage error (i.e., $V_{\text{DC}}^{*} - V_{\text{DC}}$). Then, the inversion modulation signal m_{ac} is generated by the inner proportional-resonant (PR) current controller $G_{\text{c2}}(s)$ [13].

(3) At the extra bidirectional DC-DC converter, a simple PI current controller $G_{\text{c3}}(s)$ is employed since the battery voltage is clamped, where the input is the error of the battery current (i.e., $i_{\text{B}}^{*} - i_{\text{B}}$), and the output is the duty cycle d_{B} for the bidirectional DC-DC converter.

B. Operation mode

As shown in Fig. 4, three operation modes are presented in the proposed flexible power control strategy. Fig. 4(a) shows the PV+Battery mode, where the PV array charges the battery. Therefore, the proposed control method enables only the DC-DC conversions at the PV port or the battery port, while the DC-AC part is disabled. The Battery+Grid mode is presented in Fig. 4(b), where the hybrid system acts as a typical two-stage converter. The power can bidirectionally flow between the grid and the battery, and d is equal to zero. Besides, the PV+Battery+Grid mode is the integration of the PV array, the battery, and the grid, as shown in Fig. 4(c). The power generated by the PV array can be controlled to flexibly flow into the battery and the grid. Those three operation modes are experimentally verified in the following.

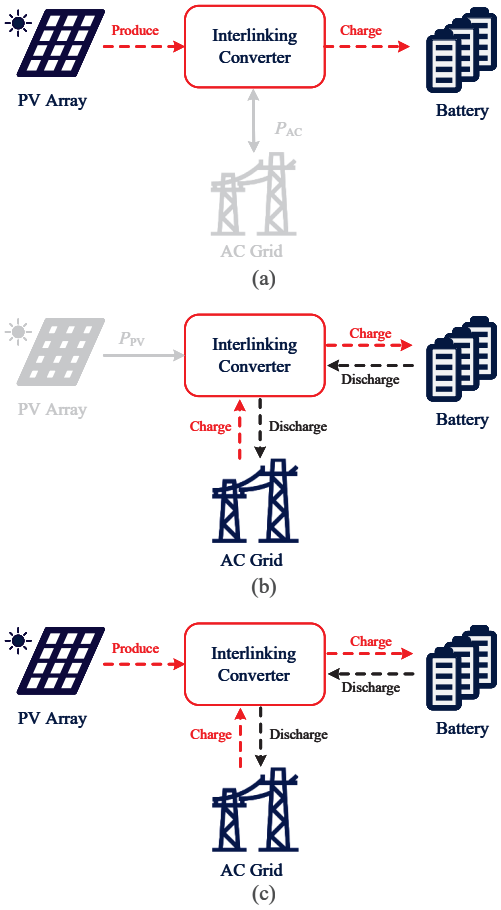

Fig. 4. Operation modes of the proposed flexible power flow control, (a) PV+Battery mode, (b) Battery+Grid mode, and (c) PV+Battery+Grid mode.

TABLE I
SYSTEM PARAMETERS

Parameters	Symbol	Values
PV voltage	V_{PV}	40-50 V
Battery voltage	V_B	35 V
AC grid voltage (RMS)	v_{AC}	23 V
Grid frequency	f_g	50 Hz
DC port capacitors	C_1, C_2	200 μF
L-type AC inductors	L_{ac1}, L_{ac2}	0.75 mH
Switching frequency	f_s	20 kHz

IV. EXPERIMENT

In the demonstration of three operation cases, the PV port is connected to a PV simulator, the battery port is connected to a battery simulator, and the AC port is connected to the utility grid by a voltage regulator, respectively. The system parameters are in Table I. Figs. 5-7 show the experimental results of the proposed control strategy under the operation modes in Fig. 4.

Fig. 5 shows the performance of the PV+Battery mode, where the bidirectional DC-DC converter works while the hybrid converter is disabled since the PV voltage is set to be higher than the battery voltage. The reference battery current is 2 A. The battery power P_{Bat} is 71.1 W, which is a little less than the PV output power P_{PV} due to the power losses. It should be noted that the interlinking converter will operate as a boost DC-DC converter and the bidirectional DC-DC converter at the battery side will be disabled when the PV voltage is lower than the battery voltage. In that case, the conversion stage can be reduced and achieve high efficiency.

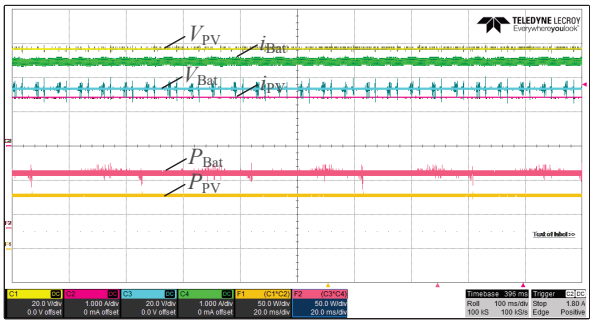

Fig. 5. Experimental result of PV+Battery mode, where P_{PV} is the product of V_{PV} and i_{PV}, and P_{Bat} is the product of V_{Bat} and i_{Bat}.

Fig. 6 is the result of the Battery+Grid mode, where Figs. 6(a) and (b) are the battery charging and discharging states, respectively. In this mode, this hybrid system likes a traditional two-stage converter, where the PV array is OFF, and the hybrid converter acts as a HERIC inverter (i.e., d being zero). The power can be flexibly controlled between the battery and the grid, where the DC-link voltage V_{DC} is controlled to be 50 V by the inverter, and the charging and discharging current is set to be 2 A. It can be seen from Fig. 6 that the interlinking converter can achieve the reactive power injection capability, providing flexible power regulation for ancillary and intelligent services in the grid-connected operation.

Furthermore, the PV+Battery+Grid mode demonstration is presented in Fig. 7, which also includes the battery charging and discharging states. When the battery is charged at 2A (see Fig. 7(a)), the PV power injects into the battery in priority, and the rest energy flows into the grid. When the battery is discharged at 2A, both the PV power and the battery power inject into the grid, as shown in Fig. 7(b). The above experimental results in Figs. 5-7 show the effectiveness of the proposed control strategy in the stand-alone interlinking converter system in terms of flexible power controllability and multifunction.

V. CONCLUSION

In this paper, a flexible power control strategy is proposed in a stand-alone hybrid converter, which interlinks the PV, the battery, and the utility grid. The hybrid system with the stand-alone interlinking converter is configured as well as proposes the control strategy and the changeable operation modes. The advantages of flexible power flow are validated through three operation modes, i.e., PV+Battery mode, Battery+Grid mode, and PV+Battery+Grid mode. Besides, it also verified that the flexible power control can enable grid-connected and off-grid

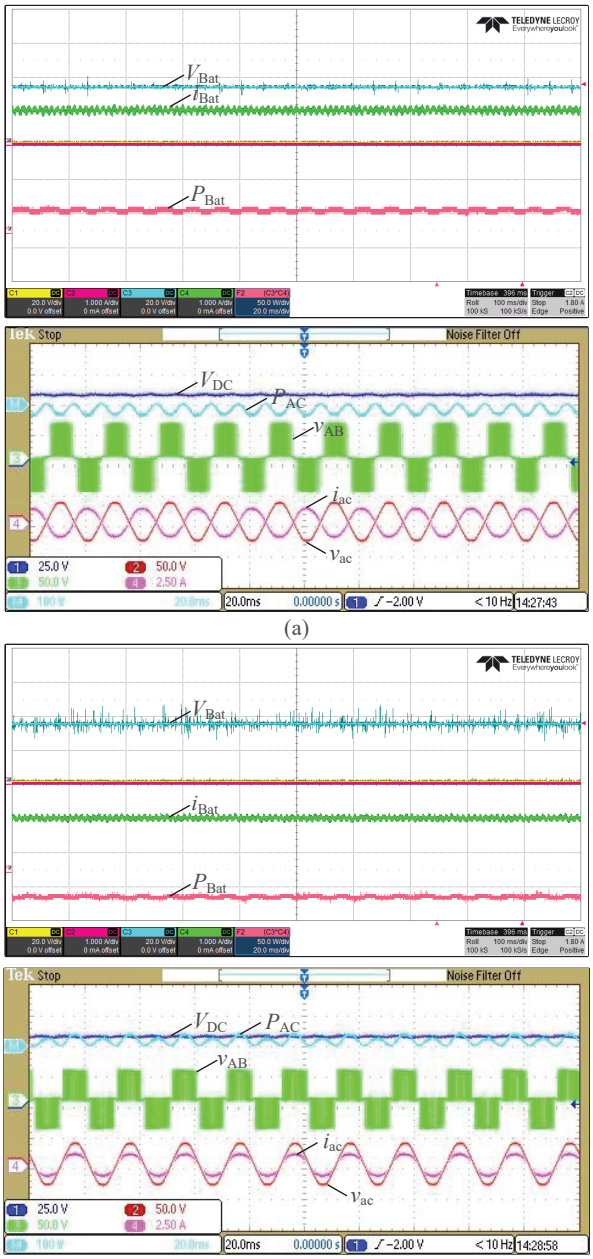

Fig. 6. Experimental results of the Battery+Grid mode, (a) Battery charging state and (b) Battery discharging state, where V_{DC}, v_{AB}, v_{ac} and i_{ac} are the DC-link voltage, the modulation voltage, the grid voltage, and the grid current, respectively, and P_{AC} is the grid power.

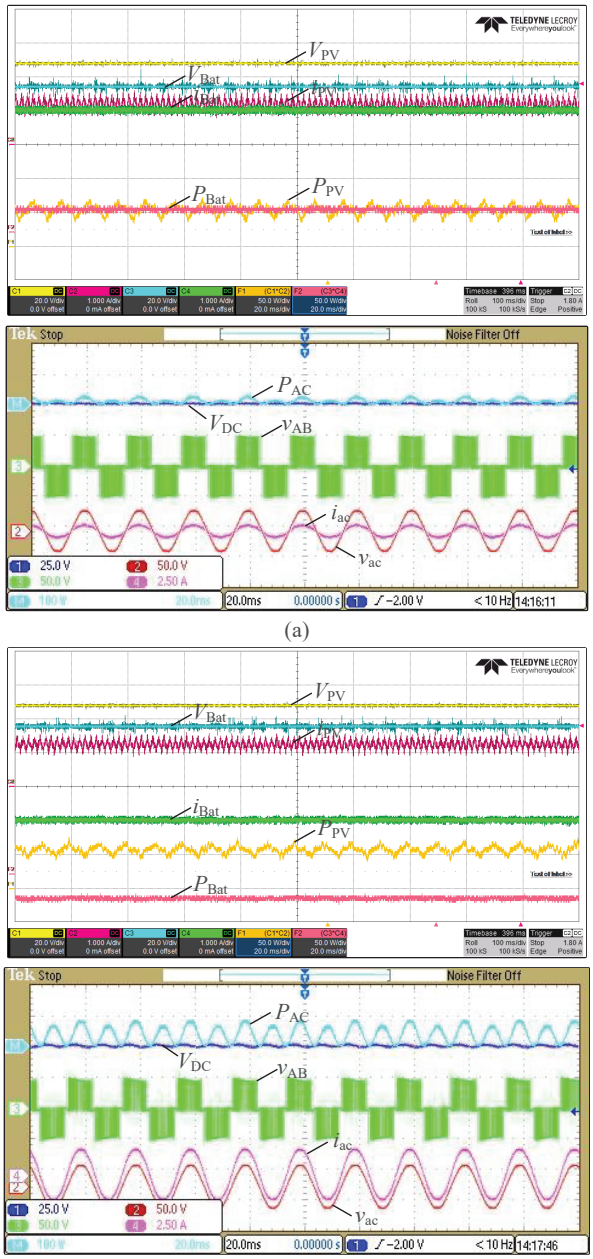

Fig. 7. Experimental test of the PV+Battery+Grid mode, (a) Battery charging state and (b) Battery discharging state.

operations of the interlinking converter. The characteristics of multifunction expand the application of the interlinking converter system in residential grid-connected renewable systems.

REFERENCES

[1] Clean Energy Reviews, Best solar inverters, Mar. 2022. [online]. https://www.cleanenergyreviews.info/blog/best-grid-connect-solar-inverters-sma-fronius-solaredge-abb.

[2] M. Ahmed, L. G. Meegahapola, M. Datta and A. Vahidnia, "A novel hybrid AC/DC microgrid architecture with a central energy storage system," *IEEE Trans. Power Deliv.*, pp. 1-1, early access.

[3] A. Gupta, S. Doolla and K. Chatterjee, "Hybrid AC–DC microgrid: systematic evaluation of control strategies," *IEEE Trans. Smart Grid*, vol. 9, no. 4, pp. 3830-3843, July 2018.

[4] S. Falcones, R. Ayyanar and X. Mao, "A DC–DC multiport-converter-based solid-state transformer integrating distributed generation and storage," in *IEEE Trans. Power Electron.*, vol. 28, no. 5, pp. 2192-2203, May 2013.

[5] Z. Tang, Y. Yang, and F. Blaabjerg, "An interlinking converter for renewable energy integration into hybrid grids," *IEEE Trans. Power Electron.*, vol. 36, no. 3, pp. 2499–2504, 2021.

[6] F. Nejabatkhah, Y. W. Li and H. Tian, "Power quality control of smart hybrid AC/DC microgrids: An oOverview," *IEEE Access*, vol. 7, pp. 52295-52318, 2019.
[7] J. M. Guerrero, M. Chandorkar, T. Lee and P. C. Loh, "Advanced control architectures for intelligent microgrids—Part I: decentralized and hierarchical control," in *IEEE Transactions on Industrial Electronics*, vol. 60, no. 4, pp. 1254-1262, April 2013.
[8] Y.-X. Dai, H. Wang, and G.-Q. Zeng, "Double closed-loop pi control of three-phase inverters by binary-coded extremal optimization," *IEEE Access*, vol. 4, pp. 7621–7632, 2016.
[9] P. C. Loh, D. Li, Y. K. Chai and F. Blaabjerg, "Autonomous control of interlinking converter with energy storage in hybrid AC–DC microgrid," *IEEE Trans. Ind. Appl.*, vol. 49, no. 3, pp. 1374–1382, May-Jun. 2013.
[10] X. Shen, D. Tan, Z. Shuai, and A. Luo, "Control techniques for bidirectional interlinking converters in hybrid microgrids: Leveraging the advantages of both ac and dc," *IEEE Power Electron. Mag.*, vol. 6, no. 3, pp. 39–47, 2019.
[11] Yang, Y., Blaabjerg, F., Wang, H., and Simões, M. G., "Power control flexibilities for grid-connected multi-functional photovoltaic inverters, " *IET Renew. Power Gener.*, vol. 10, no. 4, pp. 504-513, Apr. 2016.
[12] Z. Tang, Y. Yang and F. Blaabjerg, "A fully symmetrical three-port hybrid converter for PV systems,"in *Proc. of 2021 IEEE ECCE*, pp. 253–258, 2021.
[13] M. P. Kazmierkowski, "Modeling and control of power electronics converter system for power- quality improvements [book news]," *IEEE Ind. Electron. Mag.*, vol. 13, no. 3, pp. 52–52, 2019.
[14] M. A. G. de Brito, L. Galotto, L. P. Sampaio, G. d. A. e Melo, and C. A. Canesin, "Evaluation of the main mppt techniques for photovoltaic applications," *IEEE Trans. Ind. Electron.*, vol. 60, no. 3, pp. 1156–1167, Mar. 2013.